Modeling of combustion noise spectrum from turbulent premixed flames

Yu Liu, Ann Dowling, Thomas Dunstan, Nedunchezhian Swaminathan

ACOUSTICS 2012

Modeling of combustion noise spectrum from turbulent premixed flames

Y. Liu, A. P. Dowling, T. D. Dunstan and N. Swaminathan

University of Cambridge, Department of Engineering, Trumpington Street, CB2 1PZ Cambridge, UK
yu.liu@eng.cam.ac.uk

Turbulent combustion processes generate sound radiation due to temporal changes of the total heat release fluctuations within the flame volume. The temporal correlation of the heat release rate fluctuations has not been investigated sufficiently in prior literature due to the difficulty in acquiring heat release rate data from high-fidelity numerical simulations and measurements. In this work, this temporal correlation and its role in the modeling of combustion noise spectrum are studied by analyzing direct numerical simulation (DNS) data of turbulent premixed V-flames. The resulting correlation model is applied to the prediction of far-field combustion noise using different reference time scales. The comparison with recent measurements of open turbulent premixed flames show that the correlation model captures the essential shape of the combustion noise spectrum. Reasonable agreement in the peak frequency and peak sound pressure level (SPL) is also achieved for two turbulent time scales.

1 Introduction

Turbulent combustion processes produce sound emission due to its inherent unsteadiness. Many studies [1–4] have identified that turbulent combustion noise is generated by fluctuating heat release rate, which causes unsteady expansion of reacting gases inside the turbulent flame brush and hence behaves locally as a distributed monopole source. The focus of this paper is on direct combustion noise radiated from open turbulent premixed flames. This problem has been investigated extensively in literature but still remains a challenging issue [5] despite many efforts to develop a semi-empirical correlation for the far-field overall sound power [6, 7]. In contrast, the attention received to its spectral content is far from sufficient. Modeling the spectral characteristics of combustion noise is very challenging due to the highly nonlinear relationship between the unsteady heat release and underlying turbulent velocity fluctuations [8], and hence precise prediction models for combustion noise spectrum are not yet available. This requires a temporal correlation of the heat release rate fluctuations which has scarcely been reported in prior literature, probably due to the difficulty in acquiring heat release rate data from high-fidelity numerical simulations and measurements.

In an earlier study, Liu et al. [9] have attempted to develop a model for the two-point space-time correlation of heat release rate fluctuations by analyzing recent DNS data of turbulent premixed V-flames [10]. This two-point space-time correlation makes use of local heat release rate which undergoes abrupt variations as the flame front passes over, resulting in very high frequencies of unsteady heat release sources. Although the two-point space-time correlation has achieved success in modeling the spectrum of jet noise in non-reacting flows [11], the source mechanisms of combustion noise are more complicated due to the associated thermochemical processes and can not be described solely by local quantities. As observed by Wäsle et al. [12], turbulent combustion noise is governed by temporal changes of the total flame volume due to local heat release fluctuations. Therefore, it is the global temporal correlation of the volume integral of heat release rate fluctuations over the flame brush, denoted as the two-time correlation in this paper, that determines the spectral features.

In the present study, the V-flame DNS by Dunstan et al. [10] is rerun for a long time period to investigate this two-time correlation and its role in controlling the combustion noise spectrum. A model for the correlation function is developed from the analysis and will be used to predict the far-field SPL of combustion noise. The predictive capabilities of the correlation model will be assessed by comparing with recent measured noise data of open turbulent premixed flames [13, 8].

2 Theory

2.1 Combustion noise spectrum

Based upon the foundation laid by Lighthill's theory [14, 15], Dowling [3] has derived explicitly the sound field radiated from a turbulent reacting flow which includes a variety of source terms associated with flow noise, viscous dissipation, heat and molecular transports, direct and indirect combustion noise. The direct noise from unsteady heat input is the dominant source in most cases, and therefore the governing linear wave equation can be expressed in a reduced form as:

$$\frac{1}{a_0^2}\frac{\partial^2 p'}{\partial t^2} - \nabla^2 p' = \frac{(\gamma-1)}{a_0^2}\frac{\partial \dot{Q}'(\mathbf{y},t)}{\partial t} \tag{1}$$

for open flames where the turbulent combustion occurs at ambient pressure. In this expression, p' is the pressure perturbation, a_0 is the ambient speed of sound, γ is the ratio of specific heat capacities, respectively, and $\dot{Q}$ refers to the fluctuating rate of heat release per unit volume. For simplicity, in Eq. (1) the effects of convection due to mean flow [16] and refraction of sound due to temperature inhomogeneities [17] are neglected.

The formal solution of Eq. (1) can be written as

$$p'(\mathbf{x},t) = \frac{(\gamma-1)}{4\pi r a_0^2}\frac{\partial}{\partial t}\int_{v_f} \dot{Q}'(\mathbf{y}, t - r/a_0)\,\mathrm{d}^3\mathbf{y} \tag{2}$$

by using a free-space Green's function, where $\mathbf{x}$ denotes the observer point in far field, $\mathbf{y}$ is the source position inside the acoustically compact flame brush v_f, and $r \approx |\mathbf{x}|$ is the observer distance from an origin in v_f. It is clearly shown in Eq. (2) that the far-field sound pressure is expressed in terms of a volume integral of the unsteady heat release rate over the turbulent flame brush at a retarded time $t - r/a_0$. The source of combustion noise originates from the rate of change of this integral and behaves as an acoustic monopole. The auto-correlation function of $p'(\mathbf{x},t)$ is defined as [18]

$$P(\mathbf{x},\tau) = \frac{(\gamma-1)^2}{16\pi^2 r^2 a_0^4}\frac{\partial^2}{\partial t^2}\overline{\int_{v_f}\dot{Q}'(\mathbf{y}_a,t)\mathrm{d}^3\mathbf{y}_a \int_{v_f}\dot{Q}'(\mathbf{y}_b,t+\tau)\mathrm{d}^3\mathbf{y}_b}, \tag{3}$$

where the overbar refers to an averaging process and τ is the time lag between noise radiated from the two locations $\mathbf{y}_a, \mathbf{y}_b$ within the flame brush. The power spectral density (PSD) can be derived by a Fourier transform (FT) of Eq. (3),

$$\hat{P}(\mathbf{x},\omega) = \frac{(\gamma-1)^2\omega^2}{32\pi^3 r^2 a_0^4}\overline{\int_{v_f}\hat{\dot{Q}}(\mathbf{y}_a,\omega)\,\mathrm{d}^3\mathbf{y}_a \int_{v_f}\hat{\dot{Q}}^*(\mathbf{y}_b,\omega)\,\mathrm{d}^3\mathbf{y}_b}, \tag{4}$$

where the asterisk denotes the complex conjugate. The spectrum of the far-field combustion noise SPL, a measurable

quantity in experiments, is characterized by the PSD as $10\log_{10}(\hat{P}/p_{\text{ref}}^2)$, where the reference acoustic pressure $p_{\text{ref}} = 2\times10^{-5}$ Pa.

2.2 Two-time correlation

Following the common practice in the analysis of turbulent premixed flames [4], we use a progress variable c which varies from zero in reactants to unity in products and define the progress variable using fuel mass fraction [19]. The heat release rate $\dot{Q}$ is then related to the chemical reaction rate $\dot{w}$ as $\dot{Q} = Y_{f,u}H\dot{w}$, where the fuel mass fraction in unburnt reactants $Y_{f,u}$ is uniform in premixed cases, and H is the lower heating value of the fuel. This approximation holds good even when a complex chemical kinetics is used to model combustion [19]. In so doing, $\dot{Q}$ can be replaced by $\dot{w}$ in the analysis. The two-time correlation function is then introduced by

$$\overline{\int_{v_f}\dot{w}'(\mathbf{y}_a,t)\,\mathrm{d}^3\mathbf{y}_a\int_{v_f}\dot{w}'(\mathbf{y}_b,t+\tau)\,\mathrm{d}^3\mathbf{y}_b} = \Omega_{\text{int}}(\tau)\overline{\left(\int_{v_f}\dot{w}'(\mathbf{y},t)\,\mathrm{d}^3\mathbf{y}\right)^2}, \tag{5}$$

where all terms with overbar are independent of time t.

For the purpose of computing SPL, it is helpful to relate the correlation of the integral of reaction rate fluctuations in Eq. (5) to the mean reaction rate $\overline{\dot{w}}$ which is available from Reynolds-averaged Navier-Stokes (RANS) calculations [4],

$$\overline{\left(\int_{v_f}\dot{w}'(\mathbf{y},t)\,\mathrm{d}^3\mathbf{y}\right)^2} = \mathcal{B}_{\text{int}}^2\left(\int_{v_f}\overline{\dot{w}(\mathbf{y},t)}\,\mathrm{d}^3\mathbf{y}\right)^2, \tag{6}$$

where $\mathcal{B}_{\text{int}}$ is referred to as the "integral reaction rate intensity". This parameter does not depend on the source position according to the above definition, and its value will be worked out from the V-flame DNS data [10]. Combining Eqs. (5, 6), the two-time correlation of the integral of heat release rate fluctuations is written as

$$\overline{\int_{v_f}\dot{Q}'(\mathbf{y}_a,t)\,\mathrm{d}^3\mathbf{y}_a\int_{v_f}\dot{Q}'(\mathbf{y}_b,t+\tau)\,\mathrm{d}^3\mathbf{y}_b} = Y_{f,u}^2H^2\mathcal{B}_{\text{int}}^2\,\Omega_{\text{int}}(\tau)\left(\int_{v_f}\overline{\dot{w}(\mathbf{y},t)}\,\mathrm{d}^3\mathbf{y}\right)^2. \tag{7}$$

By substituting Eq. (7) into Eq. (3) and applying a FT, the far-field SPL of combustion noise spectrum is obtained as

$$\hat{P}(\mathbf{x},\omega) = \frac{(\gamma-1)^2}{16\pi^2r^2a_0^4}Y_{f,u}^2H^2\mathcal{B}_{\text{int}}^2\omega^2\hat{\Omega}_{\text{int}}(\omega)\left(\int_{v_f}\overline{\dot{w}(\mathbf{y},t)}\,\mathrm{d}^3\mathbf{y}\right)^2. \tag{8}$$

3 DNS and test flames

3.1 DNS V-flames

The single V-flame is one of several canonical configurations for premixed turbulent flames. Recently, DNS for laboratory-scale V-flames has become available and much progress has been made. Dunstan et al. [10] carried out three-dimensional (3D) fully compressible DNS of premixed turbulent V-flames with particular emphasis on the evaluation of turbulent flame speed. They used a cubic computation domain with the Navier-Stokes Characteristic Boundary Conditions (NSCBC) [20] in the streamwize x-direction and the transverse y-direction. The spanwize z-direction was specified to be periodic. The V-flame cases of high intensity turbulence, Case III, is selected for the analysis of the correlation functions because the faster movement of the flame front in this case is expected to produce better convergence of the correlations in time. A single-step chemical mechanism was used for preheated reactants with unity Lewis numbers in all cases. The unstrained laminar flame thermal thickness is $\delta_L = 0.43$ mm and the flame speed is $S_L = 0.6$ m s^{-1} giving a laminar flame time of $\tau_L = \delta_L/S_L = 0.71$ ms.

With respect to the spatial resolution, the computational domain has dimensions of $L_c = 12.77$ mm ($29.7\delta_L$) in each direction and is discretized using $512\times512\times512$ uniform grid, ensuring a minimum of about 10 grid points inside the laminar flame thickness δ_L. While running the DNS, data were collected consecutively during one flow-through time τ_D (the mean convection time from the inlet to outlet boundaries) after the turbulence had reached a fully developed state and one time length of τ_D had been run to ensure the decay of initial transients. As for the temporal resolution, Case III has 85 uniform time steps ($\Delta t = 10^{-5}$ s). The original time length of Case III ($\tau_D = 1.19\tau_L$) is insufficient for constructing the two-time correlation, and hence it is rerun for a long time period ($\tau_D = 7.24\tau_L$) in this work but with a doubled time interval ($\Delta t = 2\times10^{-5}$ s) to reduce the data storage space. This new case is referred to here as Case IV. Complete details of the DNS V-flames can be found in Ref. [10].

The reaction rate fluctuations required to construct the two-time correlation function are calculated as follows. First, the mean reaction rate is obtained using the averaging

$$\overline{\dot{w}}(x,y) = \frac{1}{N_tN_z}\sum_{n=1}^{Nt}\sum_{k=1}^{N_z}\dot{w}(x,y;t_n,z_k), \tag{9}$$

where N_t is the number of sample fields collected over the second flow-through time in the DNS, and N_z is the number of grid points in the spanwize, periodic direction. This type of averaging helps to improve the statistical convergence for the mean values. The fluctuating reaction rate is hence calculated using $\dot{w}' = \dot{w} - \overline{\dot{w}}$ on point-by-point basis in the $\dot{w}$ fields saved at the N_t time steps. The samples for analysis are collected at points located at least δ_L apart from any boundaries of the computation domain to avoid any possible influences from the boundary conditions.

The construction of the correlation functions Ω_{int} is then straightforward following Eq. (5). First the reaction rate fluctuations $\dot{w}'$ are integrated numerically over the total computation domain v_c to obtain the time trace $\dot{w}'_{\text{int}}(t)$ and then the correlation function is constructed based on $\dot{w}'_{\text{int}}(t)$,

$$\Omega_{\text{int}}(\tau) = \overline{\dot{w}'_{\text{int}}(t)\dot{w}'_{\text{int}}(t+\tau)}\Big/\overline{\dot{w}'^2_{\text{int}}(t)}. \tag{10}$$

Figure 1 compares the long time traces of $\dot{w}'^+_{\text{int}}(t^+)$ and a typical local fluctuation $\dot{w}'^+(t^+)$ from the Case IV data. Due to the counteraction among the instantaneous $\dot{w}'$ field, the amplitude of $\dot{w}'^+_{\text{int}}$ is reduced to about $|\dot{w}'^+|/30$. More significantly, in contrast to the dramatic variation of $\dot{w}'$, the temporal change of $\dot{w}'_{\text{int}}$ becomes rather slower by nearly 10 times. As a result, the correlation function based on the time trace of $\dot{w}'_{\text{int}}$ is anticipated to decay slowly, leading to a spectrum peaked at low frequencies.

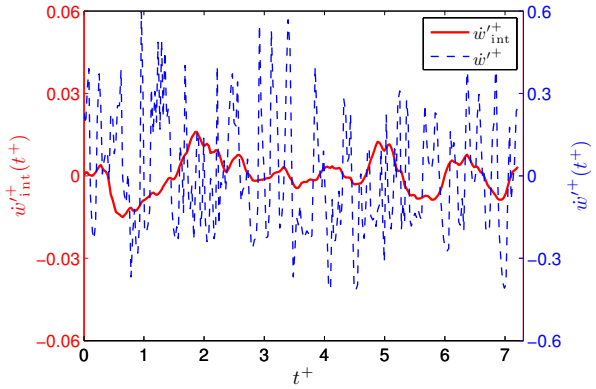

Figure 1: Time trace of $\dot{w}'^{+}_{\rm int}$ (normalized by $v_c\rho_u S_L/\delta_L$). Also plotted for comparison is the time trace of $\dot{w}'^{+}$ (normalized by $\rho_u S_L/\delta_L$) at $x_o^+ = 16.7$, $\tilde{c} = 0.5$.

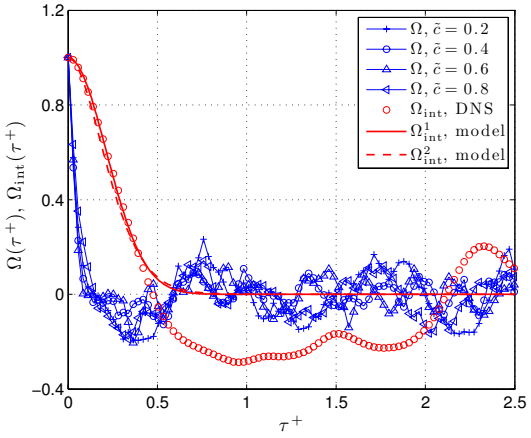

Figure 2: Temporal correlation functions $\Omega(0,\tau^+)$ and $\Omega_{\rm int}(\tau^+)$ from the DNS data together with the two models for the two-time correlation function.

3.2 Test flames

Recently, Rajaram [13] and Rajaram & Lieuwen [8] reported measurements of the far-field noise spectrum from statistically stationary, pilot stabilized, turbulent premixed flames. These axisymmetric flames with burner diameter D cover a wide range of turbulence and thermo-chemical conditions in terms of turbulence intensity, mean burner exit velocity, fuel type, equivalence ratio, etc. In the present study, twelve natural gas- and propane-air flames are selected arbitrarily out of the large database of flame conditions obtained by Rajaram [13], and will be used for the SPL prediction. The combustion noise level was measured in the far field at $r = 1.02$ m in an anechoic facility. The maximum error in the measured SPL is estimated to be about ±2.2 dB with an average bias error due to acoustic reflection ~ 1.5 dB in the frequency range of 100–500 Hz, yielding the aggregate error of about ±3.7 dB at the low frequencies. This bias error causes undulations in the measured spectra particularly the low-frequency side. The peak frequency $f_{\rm peak}$ was then determined by a fourth-order polynomial curve fitting through the noise spectrum near $f_{\rm peak}$ to minimize the room reflection effect. The uncertainty in the resulting peak frequency of the curve-fitted spectrum was estimated to be approximately ±30 Hz for $f_{\rm peak} < 400$ Hz. Further details of these test flames can be found in Ref. [13].

4 Results and discussion

4.1 Correlation function and model

Previous studies on combustion noise [4, 9] and jet noise [11] have indicated that the correlation of the noise sources can be represented reasonably well by a Gaussian-type function. Similarly, the Gaussian functions are employed and two model forms are proposed for the two-time correlation function $\Omega_{\rm int}(\tau^+)$, i.e.

$$\text{Model 1}: \qquad \Omega^1_{\rm int}(\tau^+) = \exp\left(-a\pi\tau^{+2}\right), \tag{11}$$

$$\text{Model 2}: \quad \Omega^2_{\rm int}(\tau^+) = \exp\left[-c_1\pi\tau^+/\left(1+c_2\tau^{+-1}\right)\right]; \tag{12}$$

where the superscript + denotes a normalization process based on a reference time scale; the coefficients a, c_1, c_2 represent the decay rate of $\Omega_{\rm int}$. The purpose of the variant form of Model 2 is to accurately model the shape of combustion noise spectrum in the high-frequency range.

Consider first the laminar flame time scale τ_L for which the coefficients in the correlation models take the values $a = 3.5$ and $c_1 = 5.0, c_2 = 1.0$. Figure 2 shows the results of the two-time correlation function $\Omega_{\rm int}(\tau^+)$ together with those of the two-point temporal correlation function $\Omega(0,\tau^+)$ for comparison. It is evident that $\Omega_{\rm int}(\tau^+)$ decays much more slowly than $\Omega(0,\tau^+)$, as expected, because of the slower variation of the time trace of the volume-integrated quantity $\dot{w}'_{\rm int}(t)$ compared with the dramatic local fluctuations $\dot{w}'(\mathbf{y},t)$ as have been shown in Figure 1. The DNS value of $\Omega_{\rm int}$ reaches zero around $\tau^+ = 0.5$, about 5 times larger than the corresponding value of τ^+ for Ω.

The solid and dashed lines represent the curve fits of $\Omega_{\rm int}(\tau^+)$ using the two model forms. The two curve fits show negligible difference particularly in the region $\tau^+ > 0.8$ where $\Omega_{\rm int} \to 0$; both models fit the DNS data reasonably well for small time $\tau^+ < 0.5$. The negative values and oscillations of the DNS $\Omega_{\rm int}$ at larger values of τ^+ could be ascribed to the insufficient length of running time for the V-flame Case IV. Although an enlarged sample size for averaging will improve the convergence of $\Omega_{\rm int}$ to zero, an even longer data-collecting time than the current time period $\tau^+_D = 7.24$ would be extremely expensive for the DNS of turbulent flames. Therefore the correlation model of $\Omega_{\rm int}(\tau^+)$ derived from the DNS results of Case IV will be used in the present analysis.

4.2 Prediction of noise spectrum

The comparison of noise spectrum between prediction and measurement includes two major aspects: 1) the spectral shape, in particular the low- and high-frequency dependencies $f^{\beta}, f^{-\alpha}$; and 2) the peak frequency and peak SPL. Consider first the spectral shape which has yet been fully captured in previous theoretical studies. As shown in Figure 3, the 12 noise spectra collapse reasonably well with normalized axes, i.e. the frequency and SPL are scaled by $f_{\rm peak}$ and $\text{SPL}_{\rm peak}$ respectively. The relatively large difference on the low-frequency side $f < f_{\rm peak}$ is caused by the effect of room reflections and the high background noise level in this spectrum range. Due to this signal-to-noise problems, it

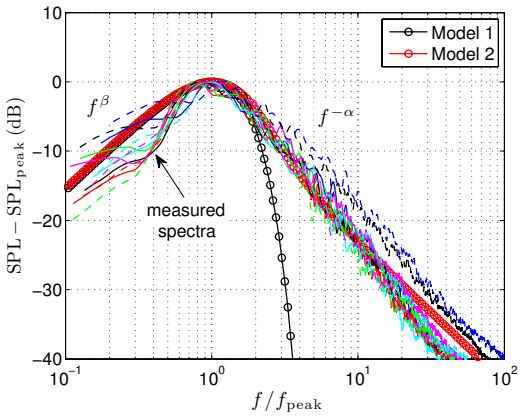

Figure 3: Measured noise spectra for the 12 test flames [13] with normalized axes, and the predicted spectral shape using the two models of the two-time correlation function $\Omega_{\rm int}$.

is most challenging to accurately measure the characteristics of the low-frequency spectrum. Rajaram & Liewen [8] first attempted to determine the low-frequency slope β by using a linear curve fit for cases with $f_{\rm peak} > 600$ Hz. They estimated that β has a nearly constant value of 2–2.4 with an uncertainty ± 0.3 at $f_{\rm peak} = 600$ Hz. The predicted spectral shape of $\omega^2 \cdot \hat{\Omega}_{\rm int}(\omega)$ is also shown in Figure 3 for comparison. On the low-frequency side, it exhibits a reasonable agreement with the measured data and a negligible difference between the two models of $\Omega_{\rm int}$. It is observed that the measured β values in Figure 3 can be less than 2. This is because the peak frequencies of the 12 test flames are all below 600 Hz and thus their slope β can deviate from the estimated range of 2–2.4 based on flames with $f_{\rm peak} > 600$ Hz.

On the high-frequency side, the shape of the noise spectra exhibits a power law dependence upon frequency $f^{-\alpha}$. In the recent experimental study by Rajaram [8], this slope was estimated to be in a range of values $\alpha = 2.1$–3.2 from a large database of turbulent flames including the 12 test flames considered in the current work. As shown in Figure 3, the two models of the two-time correlation function $\Omega_{\rm int}$ predict totally different high-frequency dependencies. The spectrum of Model 1 shows a much stronger decay rate ($\alpha \approx$ 10–15) than the values of the measurements, whereas the Model 2 spectrum matches the measured spectra remarkably well in the high-frequency range $f > f_{\rm peak}$ in term of the slope $\alpha \approx 2.5$ which is consistent with the measured range [8]. The overall agreement in spectral shape between the measurements and the prediction using Model 2 of $\Omega_{\rm int}$ is noteworthy over the entire frequency range.

Consider next the peak frequency and peak SPL. The prediction of noise spectrum using the correlation model derived from the DNS data requires a scaling of the reference time $\tau_{\rm ref}$ from the DNS V-flame to the test flames. While evaluating $f_{\rm peak}$ and SPL$_{\rm peak}$ from the prediction model (8), it is useful to multiply $\tau_{\rm ref}$ by an empirical coefficient C_τ in order to tune the predicted peak frequencies to the measured values. The tuning effect of C_τ is proportional and a unity value $C_\tau = 1$ is equivalent to no tuning used in the scaling. Moreover, it remains to attain the integral reaction rate intensity $\mathcal{B}_{\rm int}$ that also contributes to the far-field SPL predictions. In this work, the $\mathcal{B}_{\rm int}$ value is estimated as 0.0643 by analysing the V-flame DNS data and following its definition in Eq. (6).

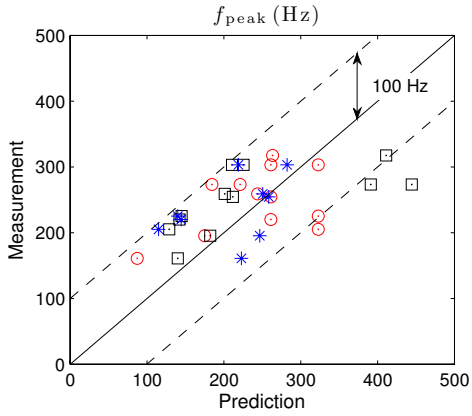

(a) peak frequency

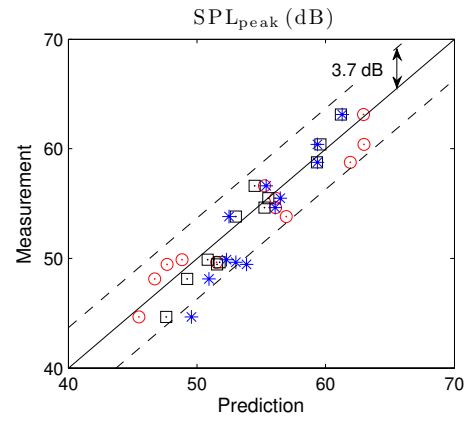

(b) peak SPL

Figure 4: Comparison of $f_{\rm peak}$ and SPL$_{\rm peak}$ between measurement and prediction for the 12 test flames [13]. Reference time scales: $\odot$ $\tau_{\rm ref} = \delta_L/S_L$, $C_\tau = 4$; $\boxdot$ $\tau_{\rm ref} = \Lambda^w/S_T^w$, $C_\tau = 1$; $\divideontimes$ $\tau_{\rm ref} = \Lambda^w/u_{\rm rms}^w$, $C_\tau = 1$.

As shown in Figure 4, the measured and predicted values of $f_{\rm peak}$ and SPL$_{\rm peak}$ are compared for the 12 test flames. The data points in circle denote the comparison for the laminar flame time scale τ_L. For this reference time scale, the tuning coefficient $C_\tau = 4$ is applied which indicates that the predicted $f_{\rm peak}$ and SPL$_{\rm peak}$ have been decreased accordingly by 4 times. After this tuning, the data points of $f_{\rm peak}$ are distributed nearly within a deviation of $\Delta_f = \pm 100$ Hz. The dashed lines in Figure 4(b) represent the error bar of $\Delta_{\rm SPL} = \pm 3.7$ dB which was estimated by Rajaram [13] as the aggregate error in the measured SPL at low frequencies $f < 500$ Hz. As can be seen from the comparison of SPL$_{\rm peak}$, the tuned data points of the reference time scale τ_L all fall into the error bars. Nevertheless, the need for a non-unity coefficient $C_\tau = 4$ indicates that the laminar flame time is incapable of characterizing the peak frequency scaling for turbulent combustion noise.

The predictive capabilities are improved by using two turbulent time scales, Λ^w/S_T^w and $\Lambda^w/u_{\rm rms}^w$, where Λ, S_T and $u_{\rm rms}$ are the turbulence integral length scale, turbulent flame speed and turbulence intensity, and the superscript w denotes the $\overline{w}$-weighted quantities. The coefficient value $C_\tau = 1$ is used in the predictions for these two turbulent time scales. As shown in Figure 4, most of the data points of $f_{\rm peak}$ and SPL$_{\rm peak}$ are confined with the deviation $\Delta_f = \pm 100$ Hz and the error bar $\Delta_{\rm SPL} = \pm 3.7$ dB. It is observed that there are 2 cases outside Δ_f for Λ^w/S_T^w and 3 cases outside Δ_f

plus 2 cases outside Δ_{SPL} for $\Lambda^w/u^w_{\mathrm{rms}}$. Nevertheless, it is noteworthy that no tuning is used (i.e. $C_\tau = 1$) in the scaling of the turbulent reference time from the DNS V-flame to the test flames, a great advantage over the laminar flame time scale for the prediction of combustion noise spectrum.

5 Conclusion

The temporal correlation of the overall change of heat release rate fluctuations within the total flame volume is crucial in predicting the spectral characteristics of combustion noise. In this study, recent high-fidelity data of 3D DNS of turbulent premixed V-flames [10] is analyzed to understand this two-time correlation and its role in controlling the combustion noise spectrum. The V-flame DNS case [10] has been rerun for a much longer time period to construct the two-time correlation function which can be modeled by a Gaussian-type function. The correlation models derived from the analyses are then applied to the prediction of the far-field noise spectrum from open flames reported by Rajaram [13]. It is found that the model reproduces the spectral shape remarkably well in terms of the excellent agreement in the low- and high-frequency dependencies (i.e. $\beta = 2.0$, $\alpha \approx 2.5$). With regard to f_{peak} and $\mathrm{SPL}_{\mathrm{peak}}$, the laminar flame time scale overestimates f_{peak} by about 4 times (tuning coefficient $C_\tau = 4$), whereas the turbulent time scales show reasonable agreement with measured data without any tuning. The predicted values of $\mathrm{SPL}_{\mathrm{peak}}$ for both laminar and turbulent time scales almost fall into the error bar $\Delta_{\mathrm{SPL}} = 3.7$ dB as estimated in Ref. [13].

Acknowledgments

The current research has been conducted under UK Technology Strategy Board contract TP11/HVM/6/I/AB201K. T.D. Dunstan and N. Swaminathan acknowledge the support of EPSRC through project EP/FO28741/1. The help of Dr. Rajaram and Dr. Lieuwen of the Georgia Institute of Technology in transferring the noise spectrum data is acknowledged.

References

[1] I. R. Hurle, R. B. Price, T. M. Sugden, and A. Thomas. Sound emission from open turbulent premixed flames. *Proc. R. Soc. Lond.*, A 303:409–427, 1968.

[2] W. C. Strahle. Combustion noise. *Prog. Energy Combust. Sci.*, 4:157–176, 1978.

[3] D. G. Crighton, A. P. Dowling, J. E. Ffowcs Williams, M. Heckl, and F. G. Leppington. *Modern Methods in Analytical Acoustics: Lecture Notes*. Springer-Verlag, London, 1992.

[4] N. Swaminathan, G. Xu, A. P. Dowling, and R. Balachandran. Heat release rate correlation and combustion noise in premixed flames. *J. Fluid Mech.*, 681:80–115, 2011.

[5] J. R. Mahan. A critical review of noise production models for turbulent, gas-fueled burners. NASA CR-3803, NASA Lewis Research Center, Ohio, USA, 1984.

[6] W. C. Strahle and B. N. Shivashankara. A rational correlation of combustion noise results from open turbulent premixed flames. *Proc. Combust. Inst.*, 15:1379–1385, 1975.

[7] A. A. Putnam. Combustion roar of seven industrial gas burners. *J. Inst. Fuel*, 49:135–138, 1976.

[8] R. Rajaram and T. Lieuwen. Acoustic radiation from turbulent premixed flames. *J. Fluid Mech.*, 637:357–385, 2009.

[9] Y. Liu, A. P. Dowling, N. Swaminathan, T. D. Dunstan, R. Morvant, M. A. Macquisten, and L. Caracciolo. Prediction of noise source for an aeroengine combustor. AIAA Paper 2011-2913, 2011.

[10] T. D. Dunstan, N. Swaminathan, K. N. C. Bray, and R. S. Cant. Geometrical properties and turbulent flame speed measurements in stationary premixed V-flames using direct numerical simulations. *Flow Turbul. Combust.*, 2010.

[11] S. A. Karabasov, M. Z. Afsar, T. P. Hynes, A. P. Dowling, W. A. McMullan, C. D. Pokora, G. J. Page, and J. J. McGuirk. Jet noise: Acoustic analogy informed by large eddy simulation. *AIAA J.*, 48(7):1312–1325, 2010.

[12] J. Wäsle, A. Winkler, and T. Sattlemayer. Spatial coherence of the heat release fluctuations in turbulent jet and swirl flames. *Flow Turbul. Combust.*, 75:29–50, 2005.

[13] R. Rajaram. *Characteristics of sound radiation from turbulent premixed flames*. PhD thesis, Department of Aerospace Engineering, Georgia Institute of Technology, Atlanta, Georgia, USA, 2007.

[14] M. J. Lighthill. On sound generated aerodynamically. I. General theory. *Proc. R. Soc. Lond.*, A 211:564–587, 1952.

[15] M. J. Lighthill. On sound generated aerodynamically. II. Turbulence as a source of sound. *Proc. R. Soc. Lond.*, A 222:1–32, 1954.

[16] A. P. Dowling. Mean temperature and flow effects on combustion noise. AIAA Paper 1979-0590, 1979.

[17] W. C. Strahle. Refraction, convection and diffusion flame effects in combustion generated noise. *Proc. Combust. Inst.*, 13:527–535, 1973.

[18] A. P. Dowling and J. E. Ffowcs Williams. *Sound and Sources of Sound*. Ellis Horwood Ltd., Chichester, England, 1983.

[19] T. J. Poinsot and D. Veynante. *Theoretical and Numerical Combustion*, chapter 1–2. Edwards Inc., Philadelphia, PA, USA, 2nd edition, 2005.

[20] T. J. Poinsot and S. K. Lele. Boundary conditions for direct simulations of compressible viscous flows. *J. Comp. Phys.*, 101:104–129, 1992.